Research article **Open Access**

Jingya Xie[a], Xinxiang Niu[a], Xiaoyong Hu*, Feifan Wang, Zhen Chai, Hong Yang and Qihuang Gong

Ultracompact all-optical full-adder and half-adder based on nonlinear plasmonic nanocavities

DOI 10.1515/nanoph-2017-0035
Received March 14, 2017; revised April 12, 2017; accepted May 17, 2017

Abstract: Ultracompact chip-integrated all-optical half- and full-adders are realized based on signal-light induced plasmonic-nanocavity-modes shift in a planar plasmonic microstructure covered with a nonlinear nanocomposite layer, which can be directly integrated into plasmonic circuits. Tremendous nonlinear enhancement is obtained for the nanocomposite cover layer, attributed to resonant excitation, slow light effect, as well as field enhancement effect provided by the plasmonic nanocavity. The feature size of the device is <15 μm, which is reduced by three orders of magnitude compared with previous reports. The operating threshold power is determined to be 300 μW (corresponding to a threshold intensity of 7.8 MW/cm^2), which is reduced by two orders of magnitude compared with previous reports. The intensity contrast ratio between two output logic states, "1" and "0," is larger than 27 dB, which is among the highest values reported to date. Our work is the first to experimentally realize on-chip half- and full-adders based on nonlinear plasmonic nanocavities having an ultrasmall feature size, ultralow threshold power, and high intensity contrast ratio simultaneously. This work not only provides a platform for the study of nonlinear optics, but also paves a way to realize ultrahigh-speed signal computing chips.

Keywords: all-optical full-adder and half-adder; plasmon-induced transparency; third-order optical nonlinearity.

1 Introduction

Nowadays, optical computing which uses photons as information carriers has attracted enormous attention, as it has the ability to support ultrahigh-speed and ultrawide-band information processing [1]. Ultracompact chip-integrated all-optical logic half- and full-adders are essential and core components in the field of optical computing system. The practical on-chip integration applications require several key indexes for these nanoscale all-optical logic devices: ultrasmall feature size, ultralow threshold power, ultrahigh contrast ratio, as well as on-chip trigger [2, 3]. More often than not, highly nonlinear fibers [4–6], optical asymmetric demultiplexers [7, 8], and bulk periodically poled lithium niobate crystals [9–11] are used to demonstrate all-optical logic functions. The large size of the bulk materials and lumped components, having a feature size of several centimeters, limits the practical on-chip integration applications [12, 13]. There are some more recent works on optical logic-/computing-related applications on different platforms, including fiber pigtail cross-section coated with a single-layer graphene [14, 15], silicon-organic hybrid slot waveguide [16], and nonlinear devices [17–19]. Subsequently, plenty of schemes have been proposed to demonstrate nanoscale all-optical logic adder based on third-order nonlinear optical effects (including cross-phase modulation) [20–24], cross-gain modulation [25–27], and four wave mixing [28–32], or linear interference mechanism [33–36]. The extremely high accuracy requirements for light paths in the linear interference configuration and relatively small third-order nonlinear susceptibility of conventional materials result in a low intensity contrast ratio of <10 dB between

[a]**Jingya Xie and Xinxiang Niu:** These authors contributed equally to this work.
***Corresponding author: Xiaoyong Hu,** State Key Laboratory for Mesoscopic Physics and Department of Physics, Collaborative Innovation Center of Quantum Matter, Peking University, Beijing 100871, P.R. China; and Collaborative Innovation Center of Extreme Optics, Shanxi University, Taiyuan 030006, P.R. China, e-mail: xiaoyonghu@pku.edu.cn
Jingya Xie, Xinxiang Niu, Feifan Wang and Zhen Chai: State Key Laboratory for Mesoscopic Physics and Department of Physics, Collaborative Innovation Center of Quantum Matter, Peking University, Beijing 100871, P.R. China
Hong Yang and Qihuang Gong: State Key Laboratory for Mesoscopic Physics and Department of Physics, Collaborative Innovation Center of Quantum Matter, Peking University, Beijing 100871, P.R. China; and Collaborative Innovation Center of Extreme Optics, Shanxi University, Taiyuan 030006, P.R. China

©2017, Xiaoyong Hu et al., published by De Gruyter.
This work is licensed under the Creative Commons Attribution-NonCommercial-NoDerivatives 3.0 License.

output logic states "1" and "0" [20–36]. Moreover, a large threshold operating intensity of several GW/cm^2 order was required for basic all-optical logic adder devices based on third-order nonlinear optical effects [20–32, 37, 38]. To the best of our knowledge, up to now, there is no experimental demonstration on complex adder device which satisfies the requirements of ultrasmall feature size, ultralow threshold power, ultrahigh contrast ratio, as well as on-chip trigger simultaneously.

Here, we propose and experimentally realize nanoscale all-optical logic full- and half-adders in nonlinear plasmonic nanostructures suitable for on-chip integration applications, based on implementing the signal-light induced shift of plasmonic nanocavity modes. The plasmonic nanostructure consisted of X-shape-crossed plasmonic slot waveguides side-coupled two plasmonic nanocavities, including a single nanocavity as well as an asymmetric composite nanocavity. A multi-component nanocomposite thin film, made of poly[2-methoxy-5-(2-ethylhexyloxy)-1,4-phenylenevinylene] (MEH-PPV) doped with organic chromophore IR140 and gold nanoflowers [nano-Au:(IR140:MEH-PPV)], was deposited on the upper surface of the plasmonic nanostructure and used as a nonlinear cover layer. The input signal light was divided into two branches equally when propagating through the crossing region, and then entered output waveguides side-coupled plasmonic nanocavities. Wang et al. and Lu et al. have noted that a composite plasmonic nanocavity could provide multiple nanocavity resonance modes [39, 40]. For a single plasmonic composite nanocavity, the plasmon-induced transparency (PIT) window could be formed by destructive interference coupling of two different nanocavity resonance modes in the composite nanocavity, called superradiant mode and subradiant mode, respectively [41, 42]. The logic operations of the full- and half-adders were performed based on the signal-light induced plasmonic-nanocavity-modes shift by using the third-order nonlinear optical Kerr effect. A large third-order optical nonlinearity was obtained for the multicomponent nano-Au:(IR140:MEH-PPV) cover layer on account of tremendous nonlinearity enhancement related to resonant excitation, slow-light effect, and field enhancement effect provided by plasmonic nanocavity modes, which cause an ultralow operating threshold power of 300 μW (corresponding to a threshold operating intensity of 7.8 MW/cm^2), reduced by two orders of magnitude compared with previous reports [20–38]. The total size of this function device is determined to be lower than 15 μm, which is reduced by three orders of magnitude compared with previously reported results [20–38]. The intensity contrast ratio between the two output logic states "1" and "0" was larger than 27 dB, which is among the highest values reported to date [20–38]. This work provides a platform for studying nonlinear optics and quantum optics, while, at the same time, paves a way to realize ultrahigh-speed signal computing chips.

2 Results and discussion

2.1 The half-adder

The half-adder which consisted of two input plasmonic waveguides A, and B, one connecting waveguide, and two output plasmonic waveguides side-coupled two plasmonic nanocavities C1 and C2 etched in a 300-nm-thick gold film deposited on a silica substrate, showing the X-shaped configuration, is shown in Figure 1A. The bending regions of the plasmonic waveguides had two quarter circular arcs with a radius of 550 nm. The nanocavity C1 was formed by two asymmetrical nanogrooves having an interval of 350 nm, both of which had the same width of 220 nm and depth of 150 nm. The length was 380 nm for the shorter one, and 430 nm for the longer one. The nanocavity C2 was formed by a single nanogroove with size parameters of 680, 220, and 150 nm for length, width, and depth, respectively. The 300-nm-thick gold film was prepared using a laser molecular beam epitaxy growth system (Model LMBE 450; SKY Company, Shenyang, China). An excimer laser system (Model COMPexPro 205, Coherent Company, Santa Clara, USA) with a beam wavelength of 248 nm, pulse width of 25 ns, and typical energy density of 430 mJ/cm^2, was chosen as the light source. Then the desired microstructure was patterned through a focused ion beam etching system (Model Helios NanoLab 600; FEI Company, Hillsboro, USA). To conveniently excite and collect the needed surface plasmon polariton (SPP) mode, we also fabricated an input-coupling grating with a depth of 300 nm connected with a 150-nm-deep triangular air groove at the input port of each plasmonic slot waveguide. For far-field signal collection and measurement, we also prepared a decoupling grating to help couple the SPP mode into free space at the terminal region of the output waveguide. The SEM image of the half-adder sample without the nano-Au:(IR140:MEH-PPV) nanocomposite cover layer is shown in Figure 1B. Finally, a 100-nm-thick nano-Au:(IR140:MEH-PPV) film was deposited onto the upper surface of the full-adder sample by using spin coating method, and the doping concentrations for IR140 and gold nanoflowers were 15% and 10%, respectively. The nanoflowers synthesized by $HAuCl_4$ have a solid core connected with plentiful pinnacles with a length ranging

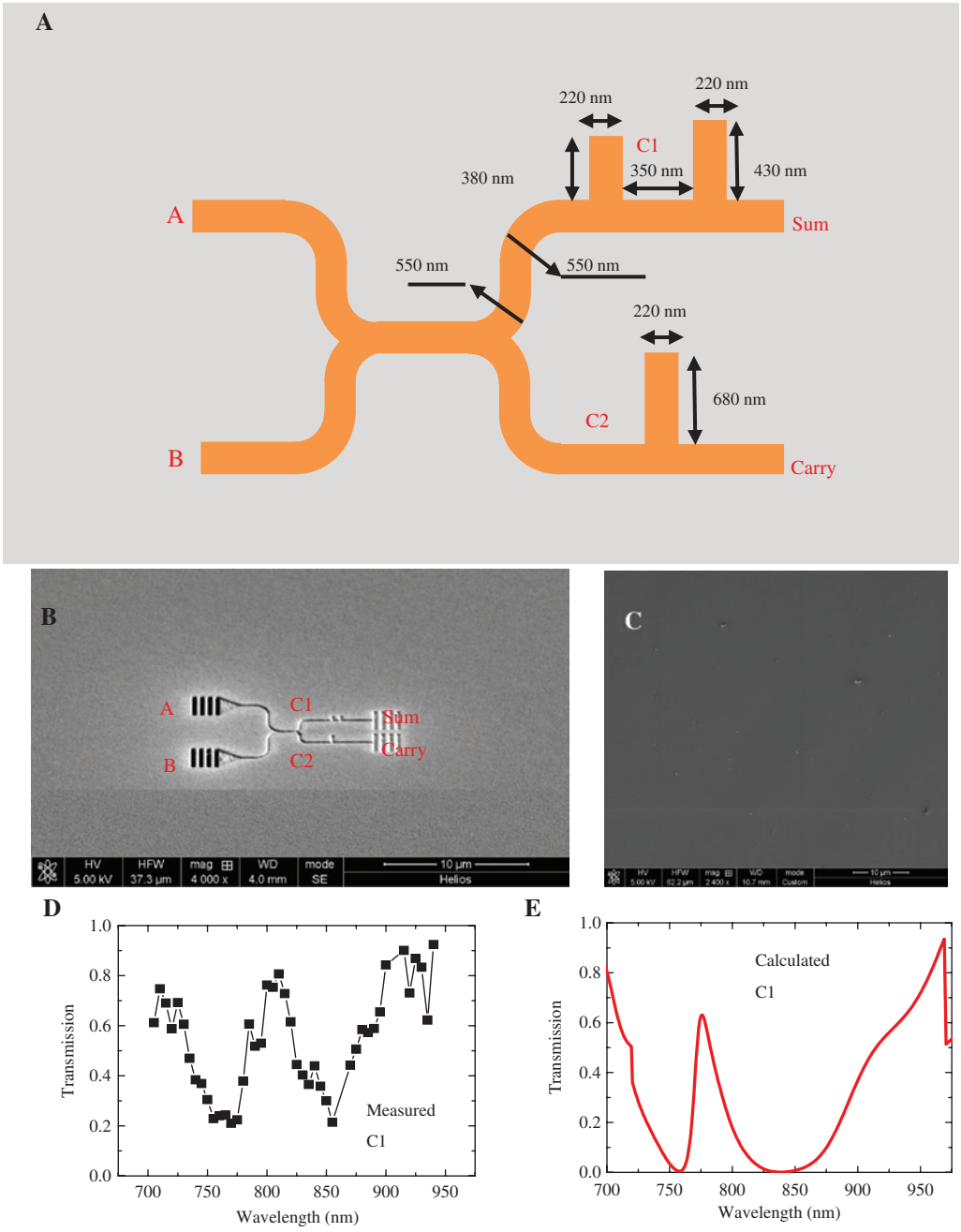


Figure 1: Characterization of the half-adder sample and performances of the logic function. (A) Schematic structure of the half-adder without the nano-Au:(IR140:MEH-PPV) nanocomposite cover layer, consisting of X-shape-crossed plasmonic waveguides side-coupled two plasmonic nanocavities etched in a 300-nm-thick gold film. (B) The SEM image of the half-adder sample without the nano-Au:(IR140:MEH-PPV) nanocomposite cover layer. (C) The SEM image of a 100-nm-thick nano-Au:(IR140:MEH-PPV) nanocomposite film. Measured (D) and calculated (E) linear transmission spectra of the plasmonic waveguide side-coupled the plasmonic composite nanocavity C1 having the nano-Au:(IR140:MEH-PPV) cover layer. Measured (F) and calculated (G) linear transmission spectra of the plasmonic waveguide side-coupled the plasmonic nanocavity C2 having the nano-Au:(IR140:MEH-PPV) cover layer. The SEM image (H) of the half-adder sample without the nano-Au:(IR140:MEH-PPV) cover layer and the measured CCD image (I) of the half-adder sample having the nano-Au:(IR140:MEH-PPV) cover layer under excitation of a 750-nm, 120-fs laser for the logic operation of "0" + "1" = (Sum "1", Carry "0"). The SEM image (J) of the half-adder sample without the nano-Au:(IR140:MEH-PPV) cover layer and the measured CCD image (K) of the half-adder sample having the nano-Au:(IR140:MEH-PPV) cover layer under excitation of a 750-nm, 120-fs laser for the logic operation of "1" + "0" = (Sum "1", Carry "0"). The SEM image (L) of the half-adder sample without the nano-Au:(IR140:MEH-PPV) cover layer and the measured CCD image (M) of the half-adder sample having the nano-Au:(IR140:MEH-PPV) cover layer under excitation of a 750-nm, 120-fs laser for the logic operation of "1" + "1" = (Sum "0", Carry "1"). Calculated linear transmission spectrum of the plasmonic waveguide side-coupled the plasmonic nanocavity C1 (N) or C2 (O) having the nano-Au:(IR140:MEH-PPV) cover layer under different excitation cases. Circles indicate which points shift to the position of 750 nm.

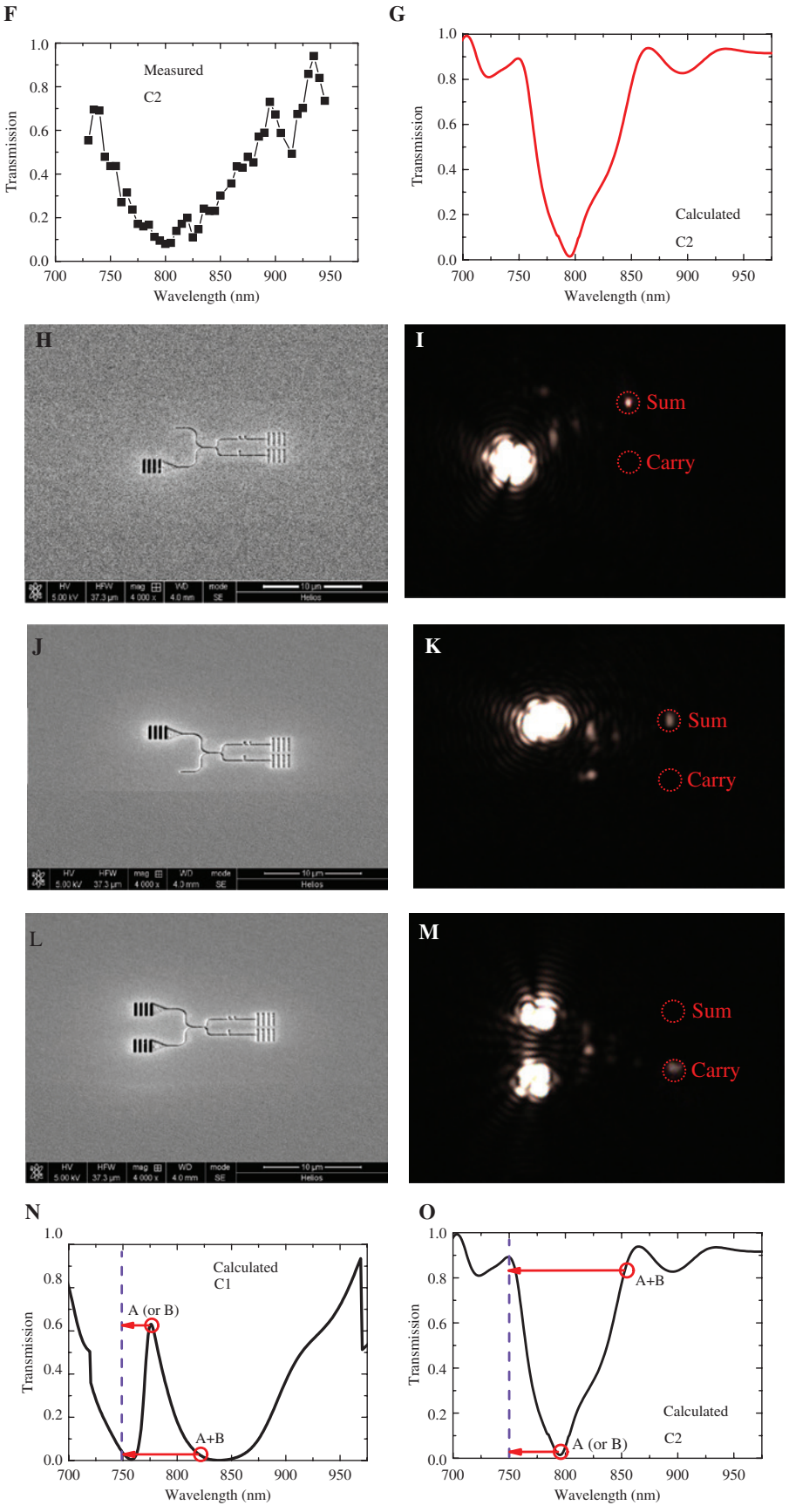


Figure 1 (continued)

from 10 to 20 nm, the size of which has a relatively large distribution [43, 44]. The SEM image for a 100-nm-thick nano-Au:(IR140:MEH-PPV) nanocomposite films deposited on a silica substrate is shown in Figure 1C. In our previous work, the linear absorption spectrum of a nano-Au:(IR140:MEH-PPV) film was measured using a visible-near-infrared absorption spectrum measurement system (LABRAM-HR800, Horiba, Japan) [43]. The results indicated that at the wavelength range from 650 to 880 nm, a linear absorption band appeared originating from the component IR140. Thus, when the wavelength of incident signal light is located near 800 nm, the third-order nonlinearity of the nanocomposite can be greatly enhanced under the circumstance of resonant excitation-enhancing nonlinearity effect and the field reinforcement effect provided by the plasmonic nanocavity mode. Moreover, the surface plasmon resonance (SPR) peak of gold nanoflowers was around 800 nm owing to a relatively large size distribution [43]. Therefore, SPR resonant excitation of gold nanoflowers contributes to the third-order optical nonlinearity reinforcement of nano-Au:(IR140:MEH-PPV) nanocomposite when the incident signal light wavelength was around 800 nm [44]. According to our previous closed-aperture Z-scan experiment, the nonlinear refractive index was measured to be -1.3×10^{-4} cm^2/kW for the nanocomposite nano-Au:(IR140:MEH-PPV) excited by a 120-fs laser beam with a wavelength around 800 nm [43], which is eight orders of magnitude larger than that of SiO_2, 1×10^{-12} cm^2/kW [45]. This means the feasibility of utilizing the nonlinear effect of nanocomposite nano-Au:(IR140:MEH-PPV) to achieve low threshold all-optical tunability.

To study the resonance properties of the plasmonic nanocavities, we measured the linear transmission spectra of the plasmonic waveguide side-coupled the plasmonic composite nanocavity C1 having the nano-Au:(IR140:MEH-PPV) cover layer by using a microspectroscopy measurement system [41]. A p-polarized CW Ti: sapphire laser system (Model Mira 900F, Coherent Company, Santa Clara, USA) was used as the incident light source. The line width of the laser spectrum was only 1.7 nm, guaranteeing that only the wanted quasi-monochromatic SPP mode could be excited and propagated in plasmonic waveguides. Incident light illuminated the input-coupling grating normally from the back side of the sample, through the transparent substrate. Due to the momentum mismatch between the SPP mode and incident light, direct propagation of the incident signal light in the plasmonic waveguide without input-coupling grating could be prohibited [46]. The SPP mode propagating through the plasmonic waveguides was scattered by using the decoupling gratings in output ports of output waveguides. The scattered light was collimated by making using of a long working distance objective (Mitutoyo 20; NA = 0.58) and then imaged by a charge-coupled device (CCD). The linear transmission was normalized with respect to a reference plasmonic waveguide without coupled nanocavity. The measured linear transmission spectrum is shown in Figure 1D. A narrow transmission peak appeared in a broad transmission forbidden band, indicating the formation of PIT transparency window, which originates from the interference coupling between two resonance modes provided by the long and short plasmonic nanogrooves [43, 44]. The central wavelength and the peak transmission of the transparency window were 800 nm and 80%, respectively, which are in agreement with the calculated one using the finite element method (employing the commercial software package COMSOL Multiphysics, Burlington, USA), as shown in Figure 1E. The complex refractive indexes of gold were extracted from the previous literature [47]. The measured linear transmission spectrum of the plasmonic waveguide side-coupled the plasmonic nanocavity C2 having the nano-Au:(IR140:MEH-PPV) cover layer is shown in Figure 1F, where a distinct dip appeared in the transmission spectrum. The minimum transmission wavelength, corresponding to the nanocavity resonance wavelength, was 800 nm, which is in good agreement with the calculated data using the finite element method, as shown in Figure 1G. To perform the logic operation of "0" + "1" = (Sum "1", Carry "0"), we etched the input-coupling grating in the input port of the plasmonic waveguide A, as shown in Figure 1H. The incident light power was also 300 μW, corresponding to a threshold intensity of 7.8 MW/cm^2. The measured CCD image of the half-adder sample having the nano-Au:(IR140:MEH-PPV) cover layer under excitation of a 750-nm, 120-fs laser is shown in Figure 1I. There was strong scattered light signal with an intensity of 27 a.u., extracted from the CCD image, from the output-coupling grating of the Sum waveguide, which corresponds to the output Sum bit "1". Very weak signal with an intensity of 0.016 a.u. was obtained from the output-coupling grating of the Carry waveguide, which corresponds to the output Carry bit "0". This means that the intensity contrast ratio between output logic states "1" and "0" reached 32.2 dB. Similar cases were obtained for the incident logic signals of ("1", "0") (shown in Figure 1J,K). These indicate that when one logic signal "1" and one logic signal "0" do half-addition operation, the Sum bit "1" and Carry bit "0" were obtained. To perform the logic operation of "1" + "1" = (Sum "0", Carry "1"), we etched the input-coupling grating in the input ports of plasmonic waveguides A, and B, as shown in Figure 1L.

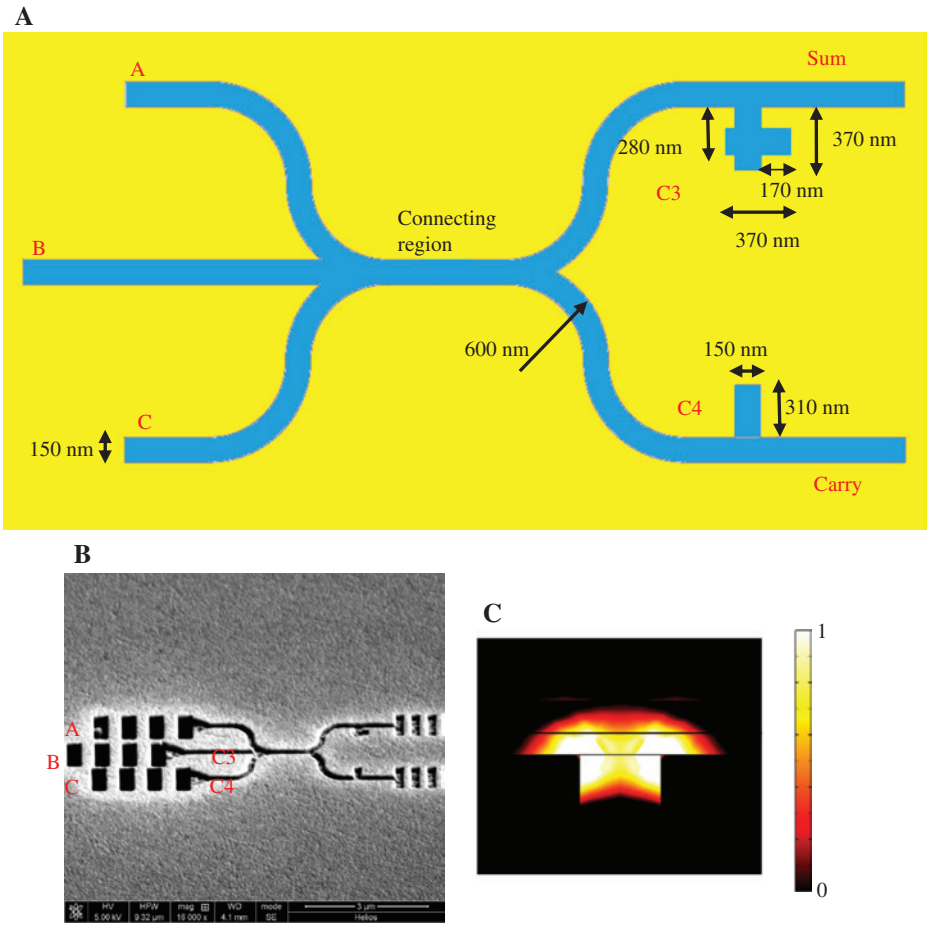


Figure 2: Configuration of the full-adder sample. (A) Schematic structure of the full-adder without the nano-Au:(IR140:MEH-PPV) nanocomposite cover layer, consisting of X-shape-crossed plasmonic waveguides side-coupled two plasmonic nanocavities etched in a 300-nm-thick gold film. (B) The SEM image of the full-adder sample without the nano-Au:(IR140:MEH-PPV) nanocomposite cover layer. (C) Calculated power density profile of the SPP mode in the plasmonic composite nanocavity C3 having the nano-Au:(IR140:MEH-PPV) cover layer under excitation of an 800-nm CW incident light.

The measured CCD image of the half-adder sample having the nano-Au:(IR140:MEH-PPV) cover layer under excitation of a 750-nm, 120-fs laser is shown in Figure 1M. There was weak scattered light signal from the output-coupling gratings of the Sum waveguide but strong scattered light signal from the output-coupling gratings of the Carry waveguide, which corresponds to the output Sum bit "0" and Carry bit "1". These means that when two logic signals "1" do half-addition operation, the Sum bit "0" and Carry bit "1" were obtained. Therefore, excellent logic operations of half-adder were achieved with an ultralow operating threshold intensity of 7.8 MW/cm^2 [48–50].

To understand the physical mechanism, we calculated the linear transmission spectrum of the plasmonic waveguide side-coupled plasmonic nanocavity C1 having the nano-Au:(IR140:MEH-PPV) cover layer under different excitation conditions, and the calculated results are shown in Figure 1N. When the signal light was incident in only one plasmonic waveguide, the transparency window center shifted to the position of 750 nm, which indicates a high transmission for the signal light, corresponding to a Sum bit of "1". When the signal light was incident in two plasmonic waveguides, the transmission minimum in the long-wavelength direction of the transmission spectrum shifted to the position of 750 nm, which indicates a low transmission for the signal light, corresponding to a Sum bit of "0". We also calculated the linear transmission spectrum of the plasmonic waveguide side-coupled plasmonic nanocavity C2 having the nano-Au:(IR140:MEH-PPV) cover layer under different excitation conditions, and the calculated results are shown in Figure 1O. When the signal light was incident in only one plasmonic waveguide, the transmission minimum in the transmission spectrum shifted to the position of 750 nm, which indicates a low transmission for the signal light, corresponding to a Carry bit of "0". When the signal light was incident in two plasmonic waveguides,

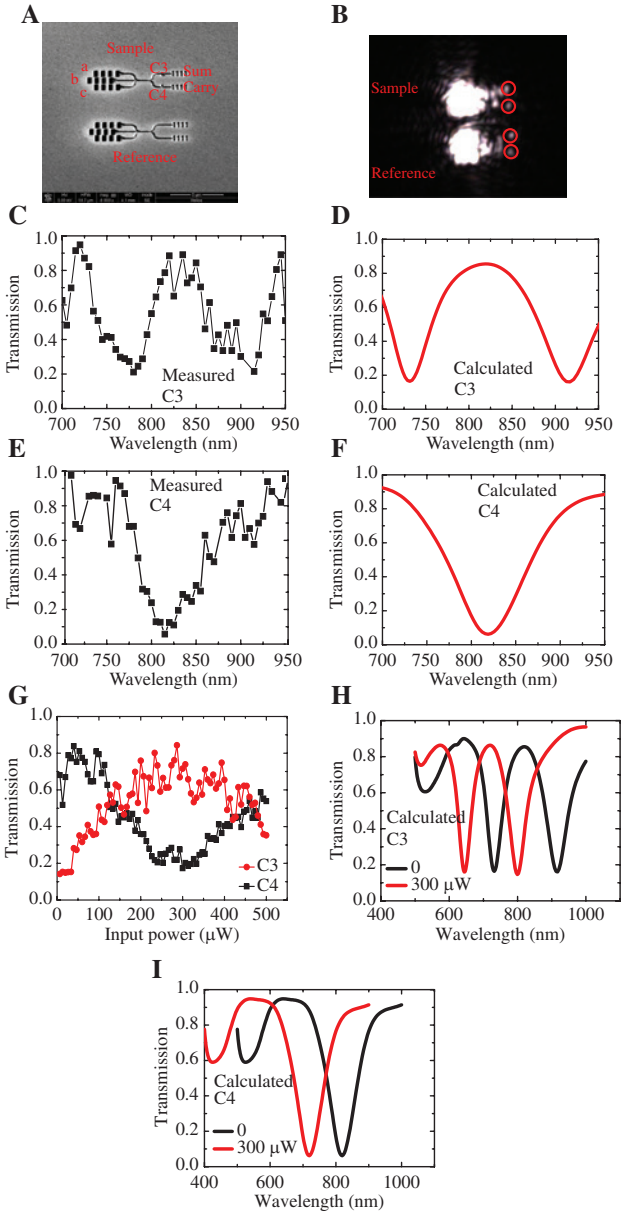


Figure 3: Characterization of the full-adder sample. (A) The SEM image of the full-adder and reference waveguides, without the nano-Au:(IR140:MEH-PPV) cover layer. (B) Measured CCD image of the full-adder sample and reference waveguides under excitation of a 730-nm CW laser beam. Measured (C) and calculated (D) linear transmission spectra of the plasmonic waveguide side coupled the plasmonic composite nanocavity C3 having the nano-Au:(IR140:MEH-PPV) cover layer. Measured (E) and calculated (F) linear transmission spectra of the plasmonic waveguide side coupled the plasmonic nanocavity C4 having the nano-Au:(IR140:MEH-PPV) cover layer. (G) Measured transmission changes of a 770-nm, 120-fs incident light propagating through the X-shape-crossed plasmonic waveguides side-coupled plasmonic nanocavities C3 (and C4) covered with the nano-Au:(IR140:MEH-PPV) cover layer as a function of the incident power. Calculated transmission spectra of the X-shape-crossed plasmonic waveguides side-coupled plasmonic nanocavities C3 (H) and C4 (I) having the nano-Au:(IR140:MEH-PPV) cover layer for different incident powers.

the pass-band in the transmission spectrum shifted to the position of 750 nm, which indicates a high transmission for the signal light, corresponding to a Carry bit of "1".

2.2 The full-adder

The full-adder which consisted of three input plasmonic waveguides A, B, and C, one connecting waveguide, and two output plasmonic waveguides side-coupled two plasmonic nanocavities C3 and C4 etched in a 300-nm-thick gold film deposited on a silica substrate, showing the X-shaped configuration, is shown in Figure 2A. The plasmonic waveguide was constructed from an air slot at the size of 150 nm for both width and depth. The bending regions of plasmonic waveguides had a configuration of quarter circular arc with a radius of 600 nm to reduce propagation losses [51]. The nanocavity C3 was formed by two orthometric asymmetrical nanogrooves, both of which have the same length of 370 nm, width of 150 nm, and depth of 150 nm. Two centers of the horizontal and vertical nanogrooves have a distance of 20 nm in the vertical direction and 15 nm in the horizontal direction. The nanocavity C4 was formed by a single nanogroove with size parameters of 310, 150, and 150 nm for length, width and depth, respectively. The SEM image of the fabricated full-adder sample without the nano-Au:(IR140:MEH-PPV) cover layer is shown in Figure 2B. To identify the guided SPP modes, we calculated the power density profile of the plasmonic nanocavity C4 mode under the excitation of an 800-nm CW light via the finite element method. The calculated results were shown in Figure 2C. The guided SPP mode was mainly confined in the nanogroove region, while also extended into the upper multicomponent nanocomposite cover layer, which agrees well with the calculated results of Li et al. [52]. This profile of field distribution leads to the characteristic that the resonance modes in plasmonic nanocavity are very sensitive to the refractive index change of the nonlinear nanocomposite cover layer.

To study the transmission properties of the plasmonic waveguides side-coupled plasmonic nanocavities C3 and C4, we measured the linear transmission spectra of plasmonic waveguides side-coupled plasmonic nanocavities C3 and C4 (Figure 3A) covered by the nano-Au:(IR140:MEH-PPV) layer by using a microspectroscopy measurement system. The measured CCD image of the structure under excitation of a 730-nm CW laser beam is shown in Figure 3B. Evident scattered light was obtained utilizing the decoupling grating. This method is widely used to study the transmission properties of plasmonic nanostructures

and is regarded as a standard [53]. Limited by the working wavelength range of the Ti: sapphire laser source, we only measured the linear transmission spectrum ranging from 700 to 950 nm. The measured linear transmission spectrum of the plasmonic waveguide side-coupled the plasmonic composite nanocavity C3 having the nano-Au:(IR140:MEH-PPV) cover layer is shown in Figure 3C, from which a sharp and high transmission peak appeared in a broad transmission forbidden band, indicating the formation of plasmon-induced transparency (PIT) window. This phenomenon could be contributed to the interference coupling between superradiant and subradiant modes provided by the composite nanocavity [43, 44]. The central wavelength and the peak transmission of the transparency window were 820 nm and 82%, respectively, which are in agreement with the calculated one using the finite element method, as shown in Figure 3D. The measured linear transmission spectrum of the plasmonic waveguide side-coupled the plasmonic nanocavity C4 having the nano-Au:(IR140:MEH-PPV) cover layer is shown in Figure 3E, where a distinct dip appeared in the transmission spectrum. The wavelength of minimum transmission, 820 nm, corresponds to the nanocavity resonance wavelength, which is in good agreement with the calculated data (Figure 3F) using the finite element method. To study the all-optical tunability of the plasmonic nanocavity resonance mode, we measured transmission changes of the 770-nm, 120-fs signal light as a function of incident power, and the measured results are shown in Figure 3G. The pulse repetition rate of the laser beam output from the Ti: sapphire laser system was 76 MHz. The wavelength of 770 nm was located in the transmission minimum in the linear transmission spectrum of the plasmonic waveguide side-coupled the plasmonic nanocavity C3, while, at the same time, this wavelength also dropped in the pass band in the linear transmission spectrum of the plasmonic waveguide side-coupled the plasmonic nanocavity C4. As the incident power increased from 50 to 300 μW, the transmission increased from 15% to 80% for the 770-nm signal light propagating through the plasmonic waveguide side-coupled plasmonic nanocavity C3, while the transmission decreased from 81% to 20% for the 770-nm signal light propagating through the plasmonic waveguide side-coupled plasmonic nanocavity C4. According to the third-order nonlinear Kerr effect, the effective refractive index n of the nano-Au:(IR140:MEH-PPV) cover layer could be expressed as [43, 44]

$$n = n_0 + n_2 I \tag{1}$$

where n_0 and n_2 represent linear and nonlinear refractive indexes of nano-Au:(IR140:MEH-PPV), and I is the intensity of pump light. Owing to the negative value of the nonlinear refractive index n_2, the refractive indexes of nano-Au:(IR140:MEH-PPV) decreased with the increase in the incident light power. As a result, the resonant modes of plasmonic nanocavities C3 and C4 shifted in the short-wavelength direction. Accordingly, the transparency window provided by C3 shifted to the short wavelength direction, and subsequently, the incident light transmission increased. When the incident power was 300 μW, the PIT window center moved to the wavelength of 770 nm, as shown in Figure 3H. When the incident light power was larger than 300 μW, the signal light transmission decreased, because the PIT window center gradually moved away from the wavelength of 770 nm. Similarly, when the incident power was 300 μW, the plasmonic nanocavity C4 mode center moved to the wavelength of 770 nm, as shown in Figure 3I, which leads to a minimum transmission of the signal light. When the incident light power was larger than 300 μW, the signal light transmission increased, because the plasmonic nanocavity C4 mode gradually moved away from the wavelength of 770 nm. These imply extraordinary all-optical tunability for plasmonic nanocavities C3 and C4 under excitation of the incident signal light.

To perform the logic operation of the full-adder sample for three single-bit logic signals, we set the output signal from the plasmonic waveguide side-coupled the plasmonic nanocavity C3 as the Sum bit, while the output signal from the plasmonic waveguide side-coupled the plasmonic nanocavity C4 as the Carry bit. To perform the logic operation of "0" + "0" + "1" = (Sum "1", Carry "0"), we etched the input-coupling grating in the input port of the plasmonic waveguide C, as shown in Figure 4A. The incident light power was 300 μW, corresponding to a threshold intensity of 7.8 MW/cm^2. The measured CCD image of the full-adder sample having the nano-Au:(IR140:MEH-PPV) cover layer under excitation of a 770-nm, 120-fs laser is shown in Figure 4B. There was strong scattered light signal with an intensity of 24 a.u., extracted from the CCD image, from the output-coupling grating of the Sum waveguide, which corresponds to the output Sum bit "1." Very weak signal with an intensity of 0.037 a.u. was obtained from the output-coupling grating of the Carry waveguide, which corresponds to the output Carry bit "0." This means that the intensity contrast ratio between output logic states "1" and "0" reached 28.1 dB. The similar cases were obtained for the incident logic signals of ("0", "1", "0") (shown in Figure 4C,D), and ("1", "0", "0") (shown in Figure 4E,F). These indicate that when one logic signal "1" and two logic signals "0" do full-addition operation, the Sum bit "1" and Carry bit "0" were obtained. To perform the logic operation of "1" + "1" + "0" = (Sum "0",

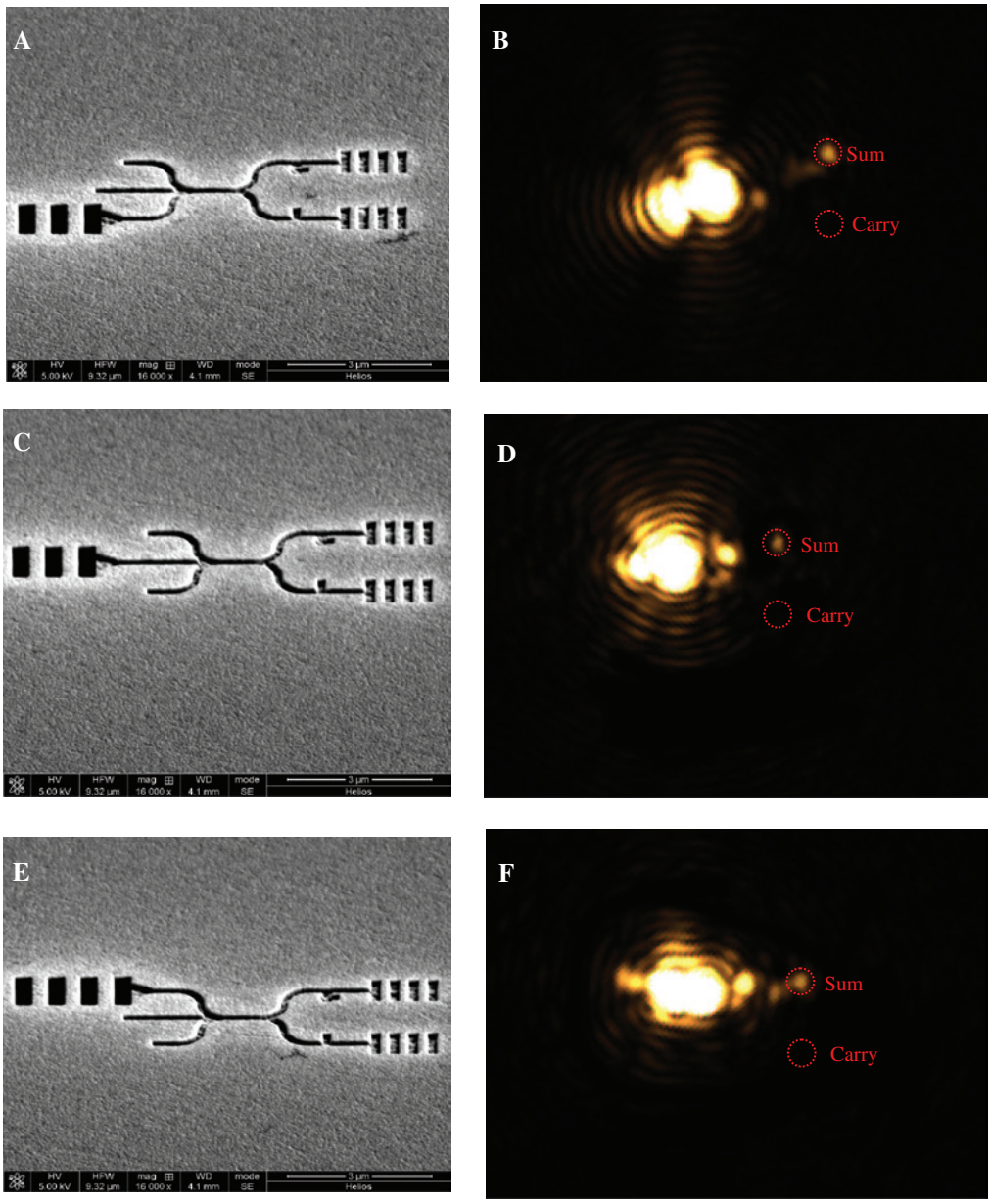


Figure 4: Performances of the logic function of the full-adder sample. The SEM image (A) of the full-adder sample without the nano-Au:(IR140:MEH-PPV) cover layer and the measured CCD image (B) of the full-adder sample having the nano-Au:(IR140:MEH-PPV) cover layer under excitation of a 770-nm, 120-fs laser for the logic operation of "0" + "0" + "1" = (Sum "1", Carry "0"). The SEM image (C) of the full-adder sample without the nano-Au:(IR140:MEH-PPV) cover layer and the measured CCD image (D) of the full-adder sample having the nano-Au:(IR140:MEH-PPV) cover layer under excitation of a 770-nm, 120-fs laser for the logic operation of "0" + "1" + "0" = (Sum "1, Carry "0"). The SEM image (E) of the full-adder sample without the nano-Au:(IR140:MEH-PPV) cover layer and the measured CCD image (F) of the full-adder sample having the nano-Au:(IR140:MEH-PPV) cover layer under excitation of a 770-nm, 120-fs laser for the logic operation of "0" + "0" + "1" = (Sum "1", Carry "0"). The SEM image (G) of the full-adder sample without the nano-Au:(IR140:MEH-PPV) cover layer and the measured CCD image (H) of the full-adder sample having the nano-Au:(IR140:MEH-PPV) cover layer under excitation of a 770-nm, 120-fs laser for the logic operation of "1" + "1" + "0" = (Sum "0", Carry "1"). The SEM image (I) of the full-adder sample without the nano-Au:(IR140:MEH-PPV) cover layer and the measured CCD image (J) of the full-adder sample having the nano-Au:(IR140:MEH-PPV) cover layer under excitation of a 770-nm, 120-fs laser for the logic operation of "1" + "0" + "1" = (Sum "0", Carry "1"). The SEM image (K) of the full-adder sample without the nano-Au:(IR140:MEH-PPV) cover layer and the measured CCD image (L) of the full-adder sample having the nano-Au:(IR140:MEH-PPV) cover layer under excitation of a 770-nm, 120-fs laser for the logic operation of "0" + "1" + "1" = (Sum "0", Carry "1"). The SEM image (M) of the full-adder sample without the nano-Au:(IR140:MEH-PPV) cover layer and the measured CCD image (N) of the full-adder sample having the nano-Au:(IR140:MEH-PPV) cover layer under excitation of a 770-nm, 120-fs laser for the logic operation of "1" + "1" + "1" = (Sum "1", Carry "1"). Calculated linear transmission spectrum of the plasmonic waveguide side-coupled the plasmonic nanocavity C3 (O) or C4 (P) having the nano-Au:(IR140:MEH-PPV) cover layer under different excitation cases. Circles indicate which points shift to the position of 770 nm.

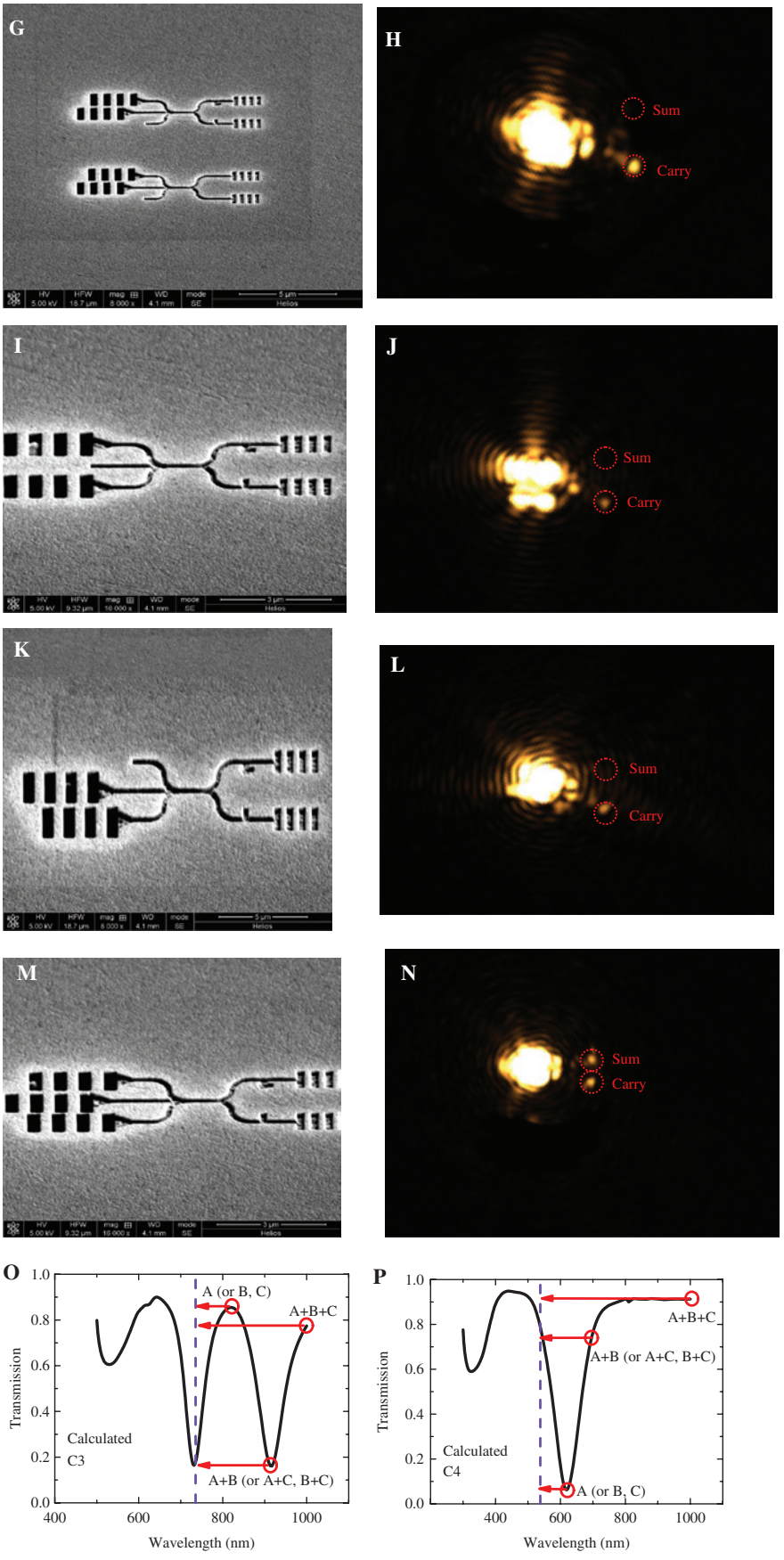


Figure 4 (continued)

Carry "1"), we etched the input-coupling grating in the input ports of plasmonic waveguides A and B, as shown in Figure 4G. The measured CCD image of the full-adder sample having the nano-Au:(IR140:MEH-PPV) cover layer under excitation of a 770-nm, 120-fs laser is shown in Figure 4H. Very weak scattered light signal with an intensity of 0.049 a.u. was obtained from the output-coupling grating of the Sum waveguide, which corresponds to the output Sum bit "0". While strong signal with an intensity of 29 a.u. was obtained from the output-coupling grating of the Carry waveguide, which corresponds to the output Carry bit "1". This means that the intensity contrast ratio between output logic states "1" and "0" reached 27.7 dB. The similar cases were obtained for the incident logic signals of ("1", "0", "1") (shown in Figure 4I,J), and ("0", "1", "1") (shown in Figure 4K,L). These indicate that when one logic signal "0" and two logic signals "1" do full-addition operation, the Sum bit "0" and Carry bit "1" were obtained. To perform the logic operation of "1" + "1" + "1" = (Sum "1", Carry "1"), we etched the input-coupling grating in the input ports of plasmonic waveguides A, B, and C, as shown in Figure 4M. The measured CCD image of the full-adder sample having the nano-Au:(IR140:MEH-PPV) cover layer under excitation of a 770-nm, 120-fs laser is shown in Figure 4N. There was strong scattered light signal from the output-coupling gratings of the both the Sum and Carry waveguides, which corresponds to the output Sum bit "1" and Carry bit "1". These means that when three logic signals "1" do full-addition operation, the Sum bit "1" and Carry bit "1" were obtained. Therefore, excellent logic operations of full-adder were achieved with an ultralow operating threshold intensity of 7.8 MW/cm^2, which is reduced by two orders of magnitude compared with previous reports [20–38]. The feature size of this function device is determined to be <15 μm, which is reduced by three orders of magnitude compared with previously reported results [20–38]. The intensity contrast ratio between the two output logic states "1" and "0" was larger than 27 dB, which is among the highest values reported to date [20–38].

To understand the physical mechanism, we calculated the linear transmission spectrum of the plasmonic waveguide side-coupled plasmonic nanocavity C3 having the nano-Au:(IR140:MEH-PPV) cover layer under different excitation conditions, and the calculated results are shown in Figure 4O. When the signal light was incident in only one plasmonic waveguide, the transparency window center shifted to the position of 770 nm, which indicates a high transmission for the signal light, corresponding to a Sum bit of "1". When the signal light was incident in two plasmonic waveguides, the transmission minimum in the long-wavelength direction of the transmission spectrum shifted to the position of 770 nm, which indicates a low transmission for the signal light, corresponding to a Sum bit of "0". When the signal light was incident in three plasmonic waveguides simultaneously, the pass-band in the long-wavelength direction in the transmission spectrum shifted to the position of 770 nm, which indicates a high transmission for the signal light, corresponding to a Sum bit of "1". We also calculated the linear transmission spectrum of the plasmonic waveguide side-coupled plasmonic nanocavity C4 having the nano-Au:(IR140:MEH-PPV) cover layer under different excitation conditions, and the calculated results are shown in Figure 4P. When the signal light was incident in only one plasmonic waveguide, the transmission minimum in the transmission spectrum shifted to the position of 770 nm, which indicates a low transmission for the signal light, corresponding to a Carry bit of "0". When the signal light was incident in two (or three) plasmonic waveguides, the pass-band in the transmission spectrum shifted to the position of 770 nm, which indicates a high transmission for the signal light, corresponding to a Carry bit of "1".

The bit rate of operation of the all-optical logic half- and full-adders is determined by the nonlinear response time of the nanocomposite nano-Au:(IR140:MEH-PPV). We measured the femtosecond-resolution optical Kerr effect responses of a 100-nm-thick nano-Au:(IR140:MEH-PPV) film under excitation of an 770-nm, 120-fs laser beam. The measured nonlinear response time was 80 ps for nano-Au:(IR140:MEH-PPV) under resonant excitation. It is the excited-state intermolecular energy transfer pathway, i.e. energy transfer from the excited states of IR140 molecules to metal that guarantees the ultrafast response time of 80 ps for nanocomposite nano-Au:(IR140:MEH-PPV) under resonant excitation [54]. This means that the intensity contrast ratio of 27 dB between output logic states "1" and "0" could be reached at a bit rate of 12.5 Gbit/s. The difference and importance of this work lies in the following two factors: first, this work provides an effective method based on signal-light induced plasmonic-nanocavity-modes shift to realize complicated all-optical logic devices. Second, this work proposes a novel method to overcome the intrinsic bottleneck limitation of nonlinear materials of large nonlinear susceptibility contradicting ultrafast response time. Excellent scalability of the presented scheme could be reached at the optical communication range because of smaller propagation losses of SPP modes, which has been confirmed by our experimental measurements [55]. According to our measurement, the input-coupling efficiency of the input-coupling grating was 20%, corresponding to the insert loss of about 7 dB. The relatively weak output intensity

originates from the relatively low efficiency of the input- and output-coupling gratings and also ultralow operating threshold signal power of 300 μW. The ultralow operating threshold signal power also confirms the high efficiency of the demonstrated full-adder and half-adder. Owing to the limitations of the experimental condition of our laboratory, we cannot fully verify the optical logic functions of full-adder and half-adder by using the data-carrying signals. The feasibility and reliability of the nanocale-integrated photonic devices based on plasmonic microstructures have been confirmed by Leuthold's measurements [56].

3 Conclusion

In conclusion, we have experimentally realized low-power ultracompact chip-integrated all-optical logic half- and full-adders in X-shaped plasmonic microstructures covered with a nonlinear nanocomposite layer, and etched in plasmonic integrated circuits directly. The logic operations were realized based on signal-light induced plasmonic-nanocavity-modes shift. The all-optical logic half- and full-adders featured a small footprint of <15 μm, a threshold operating intensity as low as 7.8 MW/cm^2, and a high contrast ratio of over 27 dB between the two output logic states "1" and "0" simultaneously. This work not only paves the way for the realization of ultrahigh-speed information processing chips, but also provides an on-chip platform for the fundamental study of nonlinear optics.

Acknowledgments: This work was supported by the 973 Program of China under grant nos. 2013CB328704 and 2014CB921003, the National Natural Science Foundation of China under grant nos. 61475003, 11134001, 11121091, and 90921008.

References

[1] Koos C, Vorreau P, Vallaitis T, et al. All-optical high-speed signal processing with silicon–organic hybrid slot waveguides. Nat Photon 2009;3:216–19.
[2] Nikolova D, Rumley S, Calhoun D, et al. Scaling silicon photonic switch fabrics for data center interconnection networks. Opt Express 2015;23:1159–75.
[3] Peng B, Ozdemir SK, Lei FC, et al. Parity–time-symmetric whispering-gallery microcavities. Nat Phys 2014;10:394–8.
[4] Singh K, Kaur G, Singh ML. A single As_2Se_3 chalcogenide highly non-linear fiber (HNLF) based simultaneous all-optical half-adder and half-subtracter. Opt Fiber Technol 2015; 24:56–63.
[5] Vlachos K. Ultrafast time-domain technology and its application in all-optical signal processing. J Lightwave Technol 2003;21:1857–68.
[6] Singh K, Kaur G, Singh ML. Simultaneous all-optical half-adder, half-subtracter, comparator, and decoder based on nonlinear effects harnessing in highly nonlinear fibers. Opt Eng 2016;55:077104.
[7] Gayen DK, Chattopadhyay T, Bhattacharyya A, Basak S, Dey D. All-optical half-adder/half-subtractor using terahertz optical asymmetric demultiplexer. Appl Opt 2014;53:8400.
[8] Gouthaml V, Goel A, Pandey G. Design of optical switching devices using all-optical half adder based on terahertz optical asymmetric de-multiplexer. Opt Quant Electron 2016;48:351.
[9] Kumar S, Willner AE. All-optical half adder using an SOA and a PPLN waveguide for signal processing in optical networks. Opt Express 2016;14:10255–60.
[10] Wang J, Sun JQ, Sun QZ. Single-PPLN-based simultaneous half-adder, half-subtracter, and OR logic gate: proposal and simulation. Opt Express 2007;15:1690–9.
[11] McGeehan JE, Kumar S, Willner AE. Simultaneous optical digital half-subtraction and -addition using SOAs and a PPLN waveguide. Opt Express 2007;15:5543–9.
[12] Ostatnicky T, Shelykh IA, Kavokin AV. Theory of polarization controlled polariton logic gates. Phys Rev B 2010;81:125319.
[13] Singh K, Kaur G, Singh ML. A cascadable all-optical half-subtracter based on crossmodulation effects in a single highly nonlinear fiber (HNLF). Opt Quant Electron 2016;48:418.
[14] Hu X, Wang AD, Zeng MQ, et al. Graphene-assisted multiple-input high-base optical computing. Sci Rep 2016;6:32911.
[15] Wang AD, Hu X, Zhu L, Zeng MQ, Fu L, Wang J. Experimental demonstration on two-input optical high-base hybrid doubling and subtraction functions in graphene. Opt Express 2015;23:31728–35.
[16] Gui CC, Wang J. Silicon-organic hybrid slot waveguide based three-input multicasted optical hexadecimal addition/subtraction. Sci Rep 2014;4:7491.
[17] Wang J, Yang JY, Huang H, Willner AE. Three-input optical addition and subtraction of quaternary base numbers. Opt Express 2013;21:488–99.
[18] Wang J, Yang JY, Wu XX, Willner AE. Optical hexadecimal coding/decoding using 16-QAM signal and FWM in HNLFs. J Lightwave Technol 2012;30:2890–900.
[19] Wang J, Nuccio SR, Yang JY, Wu XX, Bogoni A, Willner AE. High-speed addition/subtraction/complement/doubling of quaternary numbers using optical nonlinearities and DQPSK signals. Opt Lett 2012;37:1139–41.
[20] Dorren HJS, Yang X, Mishra AK, et al. All optical logic based on ultrafast gain and index dynamics in a semiconductor optical amplifier. IEEE J Select Top Quantum Electron 2004;10:1079–92.
[21] Dai B, Shimizu S, Wang X, Wada N. Simultaneous all-optical half-adder and half-subtracter based on two semiconductor optical amplifiers. IEEE Photon Technol Lett 2013;25:91–3.
[22] Stubkjaer KE. Semiconductor optical amplifier-based all-optical gates for high-speed optical processing. IEEE J Select Top Quantum Electron 2000;6:1428–35.
[23] Liu Y, Zhang S, Ju H, et al. All-optical logic gates using semiconductor optical amplifier assisted by optical filter. Electron Lett 2005;41:1397– 99.

[24] Du Y, Zhang GP, Wu YH, et al. Proposal and investigation of photonic data selector based on cross-phase modulation in highly nonlinear fiber. Opt Fiber Technol 2013;19:40–6.
[25] Lei L, Dong J, Zhang Y, He H, Yu Y, Zhang X. Reconfigurable photonic logic full-adder and full-subtracter based on three-input XOR gate and logic minterms. Electron Lett 2012;48:399–400.
[26] Ghosh P, Kumbhakar D, Mukherjee AK, Mukherjee K. An all-optical method of implementing a wavelength encoded simultaneous binary full-adder-full subtracter unit exploiting nonlinear polarization rotation in semiconductor optical amplifier. Optik 2011;122:1757–63.
[27] Garai SK. A method of developing frequency encoded multi-bit optical data comparator using semiconductor optical amplifier. Opt Laser Technol 2011;43:124–31.
[28] Kumar S, Willner AE. Simultaneous four-wave mixing and cross-gain modulation for implementing an all-optical XNOR logic gate using a single SOA. Opt Express 2006;14:5092–7.
[29] Gui CC, Wang J. Simultaneous optical half-adder and half-subtracter using a single slot waveguide. IEEE Photonics J 2013;5:6602010.
[30] Ghosh P, Garai SK, Mukhopadhyay S. Method of developing and all optical wavelength encoded single bit comparator exploiting four-wave mixing and wavelength filtering character of nonlinear semiconductor optical amplifiers. Optik 2010;121:2230–33.
[31] Li LP, Huang DX, Zhang XL, Zhu GX. Ultrahigh-speed all-optical half adder based on fourwave mixing in semiconductor optical amplifier. Opt Express 2006;14:11839–47.
[32] Lei L, Dong J, Zou B, Wu Z, Dong W, Zhang X. Expanded all-optical programmable logic array based on multi-input/output canonical logic units. Opt Express 2014;22:9959–70.
[33] Chattopadhyay T, Das MK, Roy JN, Chakraborty AK, Gayen DK. Conversion of binary number to its quaternary signed digit form and its all-optical implementation. IET Circuits Devices Syst 2011;5:132–42.
[34] Li J, Li L, Jin L, Li C. All-optical switch and limiter based on nonlinear polarization in Mach-Zehnder interferometer coupled with a polarization maintaining fiber-ring resonator. Opt Commun 2006;260:318–23.
[35] Gayen DK, Bhattacharya A, Chattopadhyay T, Roy JN. Ultrafast all-optical half adder using quantum-dot semiconductor optical amplifier-based Mach-Zehnder interferometer. J Lightwave Technol 2012;30:3387–93.
[36] Gayen DK, Chattopadhyay T. Designing of optimized all optical half adder circuit using single quantum-dot semiconductor. J Lightwave Technol 2013;31:2029–35.
[37] Fu YL, Hu XY, Lu CC, Yue S, Yang H, Gong QH. All-optical logic gates based on nanoscale plasmonic slot waveguides. Nano Lett 2012;12:5784–90.
[38] Yang XY, Hu XY, Yang H, Gong QH. Ultracompact all-optical logic gates based on nonlinear plasmonic nanocavities. Nanophotonics 2017;6:365–76.
[39] Wang TB, Wen XW, Yin CP, Wang HZ. The transmission characteristics of surface plasmon polaritons in ring resonator. Opt Express 2009;17:24096.
[40] Lu H, Liu XM, Mao D, Wang L, Gong YK. Tunable band-pass plasmonic waveguide filters with nanodisk resonators. Opt Express 2010;18:17922.
[41] Chai Z, Hu XY, Zhu Y, Sun SB, Yang H, Gong QH. Ultracompact chip-integrated electromagnetically induced transparency in a single plasmonic composite nanocavity. Adv Opt Mater 2014;2;320–25.
[42] Kekatpure RD, Barnard ES, Cai W, Brongersma ML. Phase-coupled plasmon-induced transparency. Phys Rev Lett 2010;104:243902.
[43] Chai Z, Hu XY, Yang H, Gong QH. Chip-integrated all-optical diode based on nonlinear plasmonic nanocavities covered with multicomponent nanocomposite. Nanophotonics 2017;6:329–39.
[44] Chai Z, Hu XY, Wang FF, Niu XX, Xie JY, Gong QH. Ultrafast all-optical switching. Adv Opt Mater 2016;4:1600665.
[45] Miller A, Welford KR, Daino B. Nonlinear optical materials and devices for application in information technology, The Netherlands, Kluwer Academic, 1992.
[46] Barnes W, Dereux A, Ebbesen TW. Surface plasmon subwavelength optics. Nature 2003;424:824–30.
[47] Johnson PB, Christy RW. Optical constants of the noble metals. Phys Rev B 1972;6:4370–9.
[48] Kumar A. Implementation of all-optical NAND logic gate and half adder using the micro-ring resonator structures. Opt Quant Electron 2016;48:477.
[49] Birr T, Zywietz U, Chhantyal P, Chichkov BN, Reinhardt C. Ultrafast surface plasmon-polariton logic gates and half-adder. Opt Express 2015;23:31755–65.
[50] Kumar A, Kumar S, Raghuwanshi SK. Implementation of full-adder and full-subtractor based on electro-optic effect in Mach–Zehnder interferometers. Opt Commun 2014; 324:93–7.
[51] Volkov VS, Bozhevolnyi SI. Compact gradual bends for channel plasmon polaritons. Opt Express 2006;14: 4494–503.
[52] Li XE, Jiang T, Shen LF, Deng XH. Subwavelength guiding of channel plasmon polaritons by textured metallic grooves attelecom wavelengths. Appl Phys Lett 2013;102:031606.
[53] Han ZH, Garcia-Ortiz CE, Radko IP, Bozhevolnyi SI. Detuned-resonator induced transparency in dielectric-loaded plasmonic waveguides. Opt Lett 2016;38:875–7.
[54] Hatami S, Wurth C, Kaiser M, Leubner S, Gabriel S, Bahrig L, et al. Absolute photoluminescence quantum yields of IR 26 and IR-emissive $Cd_{1-x}Hg_xTe$ and PbS quantum dots – method- and material-inherent challenges. Nanoscale 2015;7:133–43.
[55] Wang FF, Gong ZB, Hu XY, Yang XY, Yang H, Gong QH. Nanoscale on-chip all-optical logic parity checker in integrated plasmonic circuits in optical communication range. Sci Rep 2016;6:24433.
[56] Haffner C, Heni W, Fedoryshyn Y, et al. All-plasmonic Mach-Zehnder modulator enabling optical high-speed communication at the microscale. Nat Photonics 2015;9:525–8.